

Vrancea slab earthquakes triggered by static stress transfer

A. Ganas¹, B. Grecu², E. Batsi¹, and M. Radulian²

¹Geodynamics Institute, National Observatory of Athens, 118 10 Lofos Nymfon, P.O. Box 20048, Athens, Greece

²National Institute for Earth Physics, Calugareni str. 12, P.O. MG-2, 077125, Bucharest-Magurele, Ilfov, Romania

Received: 31 March 2010 – Revised: 22 July 2010 – Accepted: 7 September 2010 – Published: 15 December 2010

Abstract. The purpose of this paper is to study the interaction of the Vrancea seismic activity (Romania) in space as result of Coulomb, static stress transfer during $M = 7+$ events. In this area, three large events occurred in 1977, 1986 and 1990 at mid-lower, lithospheric depths and with similar focal mechanisms. Assuming elastic rheology for the deforming rocks it is suggested that frictional sliding on pre-existing fault produced the 1986 $M = 7.1$ event (depth 131 km), that was possibly triggered by the 1977 $M = 7.4$ event (depth 94 km). We calculated a static stress transfer of 0.52–0.78 bar to the hypocentre of the 1986 event. On the contrary, the occurrence of the 1990 event is uncertain: it is located inside the relaxed (shadow) zone of the combined 1977 and 1986 static stress field considering an azimuth for maximum compression of N307° E. It follows that, the 1990 earthquake most likely represents an unbroken patch (asperity) of the 1977 rupture plane that failed due to loading. However, if a different compression azimuth is assumed (N323° E) then the 1990 event was also possibly triggered by static stress transfer of the 1977 and 1986 events (combined). Our modeling is a first-order approximation of the kind of earthquake interaction we might expect at intermediate lithospheric depths (80–90 to 130–140 km). It is also suggested that static stress transfer may explain the clustering of Vrancea earthquakes in space by the rupturing of two (possibly three) NW-dipping major zones of weakness (faults) which accommodate the extension (vertical elongation) of the slab.

area is located in Romania at the South-Eastern Carpathians arc bend (Fig. 1). The Carpathian orogen marks the site of an arc-continent collision that followed the subduction of an extinct ocean basin. Seismic tomography has defined a high-velocity anomaly in the upper mantle similar to those associated with subduction zones worldwide (e.g. Oncescu, 1984; Koch, 1985; Wortel and Spakman, 2000; Sperner et al., 2001). Intermediate-depth seismicity is confined to a small, roughly cylindrical and vertically elongated region beneath the southeastern corner of the mountain chain. Earthquakes occur at subcrustal depths (60–180 km) inside the descending slab of strong, possibly oceanic-type material (Wenzel et al., 1999; Tondi et al., 2009). On average, over two shocks with magnitude $M_w \sim 7$ occur per century producing a lot of casualties and severe damage. In the last fifty years, three significant events were recorded on 4 March 1977 (19:21 UTC; $M_w 7.4$), 30 August 1986 (21:28 UTC; $M_w 7.1$) and 30 May 1990 (10:40 UTC; $M_w 6.9$). The last event was followed at about one day by a second shock of magnitude $M_w 6.3$. Following those events, a 5-year, 40% probability for another strong event has been calculated by Imoto and HURUKAWA (2006).

All Vrancea events at intermediate depth occur in a compressive, thrust faulting regime. The fault plane solutions of the instrumentally recorded large earthquakes are remarkably similar. The fault planes typically strike SW-NE and dip either to the NW or to the SE (Oncescu and Bonjer, 1997; Sperner et al., 2001; Wenzel et al., 2002). In this paper we assume that the fault dip is to NW following closely the particular geometry of the foci distribution (Fig. 1) and overall slab dip direction (Sperner et al., 2001). The rake angle is roughly 90° (i.e. up dip). Under this strain regime the earthquake source volume is stretched in the vertical direction and shortened in horizontal direction (KIRATZI, 1993). These seismic domains are separated from the sub-Carpathian crust by a relatively aseismic zone between 40 km and 70 km depth which is substantiated by the Romanian seismic data (supplied by the National Institute of Earth Physics, NIEP) and

1 Introduction

The purpose of this paper is to study the interaction of the Vrancea seismic activity in space as result of Coulomb, static stress transfer during $M = 7+$ events. The Vrancea seismic



Correspondence to: A. Ganas
(aganas@gein.noa.gr)

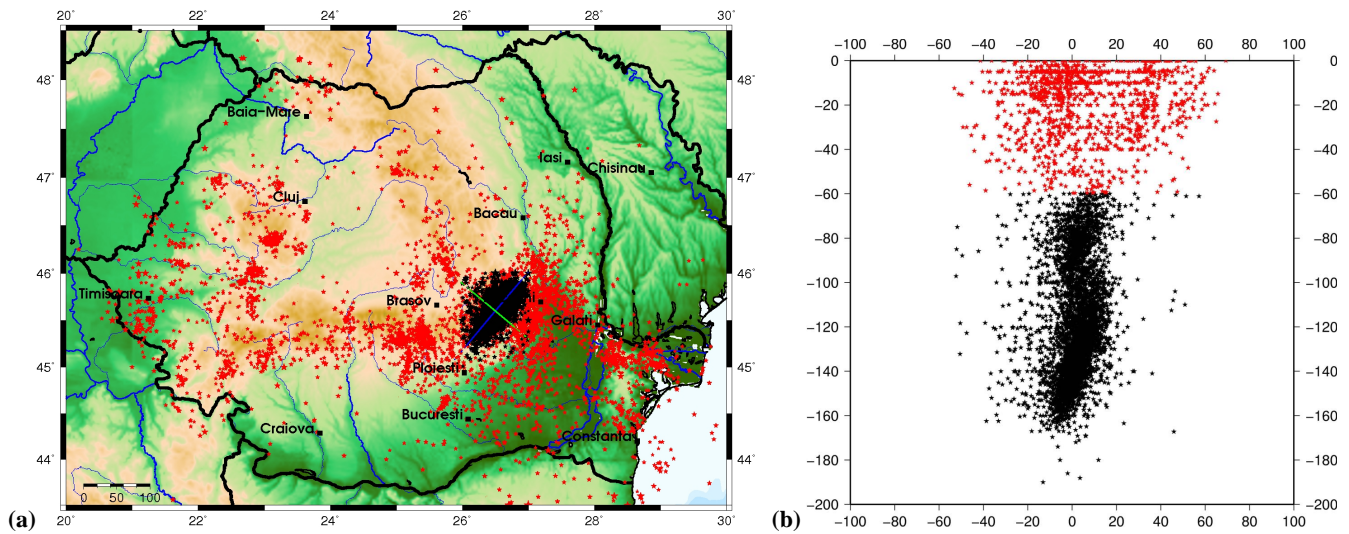


Fig. 1. (a) Map showing seismicity of the SE-Carpathians and surrounding regions during the last century (the hypocenter catalog, ROMPLUS, provided by the National Institute for Earth Physics – NIEP, was adopted for the study). Red colour shows shallow seismicity. Black colour shows intermediate-depth seismicity. Note that the main source of earthquake hazard, the intermediate-depth events, is clustered in a small elliptical-geometry area to the North of Bucharest (b) NW-SE cross section of seismicity (azimuth N130° E).

Table 1. List of earthquakes analyzed in this study. Earthquake parameters after Oncescu and Bonjer (1997). $\Delta\sigma$ is static stress drop (bar): 1977 event after Tavera (1991), 1986 event after Oncescu (1987) and 1990 event after Trifu et al. (1992).

No	Date	Latitude (° N)	Longitude (° E)	Depth (km)	Mw	$\Delta\sigma$ bar	Strike (°)	Dip (°)	Rake (°)
1	4 Mar 1977	45.77	26.76	94	7.4	44	194	41	87
2	30 Aug 1986	45.52	26.49	131	7.1	50	227	65	104
3	30 May 1990	45.87	26.87	89	6.9	110	232	58	89

possibly reflects the existence of a weak material. Oncescu et al. (1984) inverted teleseismic events recorded by the Romanian network and identified a low-velocity structure between 40 and 80 km depth. On the contrary, results of simultaneous inversion of hypocentres and P-wave velocities (Oncescu, 1984; Koch, 1985) indicate high-velocity material between 80 and 160 km depth, the level where intermediate depth seismicity is located (Fig. 1b). Also, Fan et al. (1998) with a larger set of regional earthquakes and records supports that the intermediate-depth seismogenic volume is characterised by high velocities. Figure 1b shows a cross-section of the Romanian catalogue for Vrancea which demonstrates this seismicity contrast.

The predominantly intermediate-depth seismicity in Vrancea indicates slab deformation by seismic rupture where dehydration of rocks may also play an important role (Ismail-Zadeh et al., 2000). We model stress transfer assuming that failure of the slab occurs by shear, so that the mechanics of the process can be approximated by the Okada (1992) expressions for the displacement and strain fields due to a finite rectangular source in an elastic, homogeneous and isotropic

half-space. The dimensions of the sources (faults) are defined by the empirical relationships of Wells and Copper-smith (1994), assuming a rectangular geometry. The slip models of all source faults are given in Table 1. We computed static stress changes using the DLC set of computer codes by R. Simpson (USGS). For the statistical analysis and for histograms plotting, we used the Minitab Statistical Software.

2 Stress transfer methodology

Large earthquakes on fault planes can trigger subsequent earthquakes at short distances from the hypocenter (a few fault lengths) by transferring static or dynamic stresses (e.g. Harris et al., 1995; Stein et al., 1997; Gomberg et al., 2001; Freed, 2005; Parsons et al., 2006). This interaction has been widely recognized on crustal faults. In addition, Tibi et al. (2003) presented a detailed analysis of the 19 August 2002 Tonga deep earthquake sequences (600 km depth) and showed evidence for both static and dynamic triggering. In particular, seven minutes after a magnitude 7.6 earthquake occurred at a depth of 598 km, a magnitude 7.7 earthquake

(664 km depth) occurred 300 km away, in a previously aseismic region. Tibi et al. (2003) found that nearby aftershocks of the first mainshock are preferentially located in regions where static stresses are predicted to have been enhanced by the mainshock. For Vrancea, Ledermann, and Heidbach (2007) used a 3-D finite element model and suggested that stress transfer is likely to occur, as well.

In this paper which examines Vrancea earthquake interactions, we compute the Coulomb stress change in an elastic half space (Okada, 1992) by assuming a shear modulus of 7.1×10^{10} Pa, Poisson's ratio 0.28 and effective coefficients of friction $\mu' = 0.4$ and $\mu' = 1$. The elastic parameters (shear modulus and Poisson ratio) were taken from Turcotte and Schubert (1982, p. 432), according to properties for oceanic upper mantle rocks, such as those possibly comprising the descending slab. We studied two cases of effective coefficient of friction: $\mu' = 0.4$, which is closer to friction values for major faults (Harris and Simpson, 1998) and $\mu' = 1$, which is closer to friction values on faults at large depths (e.g. Tibi et al., 2003). We also calculated Coulomb stress for the whole range of friction values ($0 < \mu' < 1.1$) as we cannot exclude the possibility that pre-existing planes of failure inside the slab may be extremely weak ($\mu' < 0.1$). We assume a constant effective coefficient of friction model along pre-existing faults inside the slab. Further details on the methodology can be found in previous works such as Ganas et al. (2005, 2008) and the mechanics are described in Appendix A.

We calculated the change in the Coulomb Failure Function (ΔCFF , or Coulomb stress), on target failure planes (Reasenber and Simpson, 1992),

$$\Delta\text{CFF} = \Delta\tau + \mu' \Delta\sigma_{\eta} \quad (1)$$

where $\Delta\tau$ is the co-seismic change in shear stress on the receiver fault and in the direction of fault slip, $\Delta\sigma_{\eta}$ is the change in the normal stress (with tension positive) and μ' is the effective (or apparent) coefficient of friction,

$$\mu' = \mu (1 - \Delta P / \Delta\sigma_{\eta}) \quad (2)$$

where μ is the coefficient of static friction and ΔP is the pore pressure change within the fault. From (2) it follows that, if $\Delta P = 0$ then $\mu' = \mu$. ΔCFF is the Coulomb stress change between the initial (ambient) stress and the final stress. If the dislocation model (Table 1) is thought of as an earthquake rupture, the ambient field is the field that existed before the earthquake and the total field is the sum of the ambient field plus the earthquake-induced stresses.

2.1 Triggering of the 1986 earthquake: calculation of ΔCFF , at depth of 131 km

We computed Coulomb stress change caused by the 1977 event on optimally oriented planes to regional compression (-500 bar). For compression azimuth we adopted the orientation of the P-axis of the focal plane solution of the 1986

event (N307° E; Table 2). Oncescu and Bonjer (1997) also provide a value of 307° as azimuth for the major axis of the strain tensor. The calculation was done at the depth of the 1986 event hypocenter (131 km). The target planes are similar in orientation to the 1986 fault plane, i.e. they strike NNE-SSW and dip either to the NW or to the SE. For $\mu' = 0.4$ the angle of failure with respect to the compression axis is 34°. For $\mu' = 1$ the angle of failure with respect to the compression axis is 22°. In other words, the dip-angle of the optimally oriented plane for failure would be 34° in the former and 22° in the latter. Notice that the dips of both NW-dipping, 1986 and 1990, faults are within the range of dip-angles 56°–68° (see Table 1 for fault plane attributes), or high-angle faults. Next we run *elfgrid* to calculate the stress tensor on a horizontal observation plane at a depth of 131 km. The output is six grids, one for each component of the tensor. Then, we calculate the change in the Coulomb Failure Function (CFF) on optimal failure planes at 131 km depth by running *stroop* (*stress_on_optimal_planes*). ΔCFF was sampled on a 200×200 km grid, with 1 km grid spacing. The amount of co-seismic displacements (down-dip and along strike) was calculated by applying the Hanks and Kanamori formula (1979) for the seismic moment – moment magnitude relation:

$$M_w = (2/3) \cdot (\log M_o - 16.05) \quad (3)$$

where M_o is the scalar moment of the best double couple in dyne-cm. Seismic moment is given by the following equation:

$$M_o = G \cdot A \cdot u \quad (4)$$

where A is fault area, G is shear modulus and u is total displacement. We assumed an area of 1500 km² (50 km long – along strike by 30 km wide – down dip rupture) which is close to the empirical estimate of Wells and Coppersmith (1994; Table 2A in their paper) for $M_w = 7.4$ ruptures along crustal faults. The difference between our estimate and that of Wells and Coppersmith (1994) is 253 km² or 16%. Given that (a) the 1977 fault length was determined independently by Oncescu and Bonjer (1997; see reference in paper) as 50 km, and (b) the rupture zone of the 1977 aftershocks was located between 90 and 110 km depths (Oncescu and Bonjer, 1997; p. 295), we think that a rupture width – surface of 30 km is more appropriate (note that the fault dip is 41°; see Table 1 of the paper).

The two components of displacement vector are calculated from the following formulas given the slip models in Table 1:

$$u_s = \cos(\text{rake}) \cdot u \quad (5)$$

$$u_d = -\sin(\text{rake}) \cdot u \quad (6)$$

We estimated an average strike-slip displacement (u_s) of 0.0694 m and a dip – slip displacement (u_d) of -1.3245 m ($-$ is for upward displacement) for a magnitude $M_w = 7.4$.

Table 2. Principal stress axes as calculated using the RAKE software (Louvari and Kiratzi, 1997). Slip models are after Tavera (1991) and the global CMT project.

Date	Depth (km)	Strike/Dip/Rake Plane 1	Strike/Dip/Rake Plane 2	P-axis azimuth	P-axis plunge	T-axis azimuth	T-axis plunge
4 Apr 1977	94	194°/41°/87°	18°/49°/93°	106°	4°	313°	86°
30 Aug 1986	131	227°/65°/104°	16°/28°/62°	307°	19°	163°	67°
30 May 1990	89	232°/58°/89°	54°/32°/92°	323°	13°	139°	77°

Table 3. Input parameters used for stress transfer modeling of the 1977 earthquake ($M = 7.4$).

Poisson ratio	0.28
Shear modulus	$G = 710\,000$ bar
Map projection	UTM zone 35
Depth of Δ CFF calculation	131 km (target is 1986 hypocenter fault)
Grid size	1 km
Effective friction coefficient (μ')	0.4 and 1
Horizontal length of rupture	50 km
Down – dip length of rupture	30 km
Strike – slip displacement	0.0694 m
Dip – slip displacement	–1.3245 m
Azimuth of compression	N307° E
Regional stress	–500 bar (compression)

We assumed a regional compression 5–10 times the static stress drop of earthquakes in Vrancea (see Table 1 for stress drop estimates). It is possible that small asperities can rupture with higher stress drops (Oth et al., 2007), however, experience with previous modelling has shown no significant difference on Coulomb stress patterns. The catalogue of the aftershocks used for our study was taken from ROMPLUS catalogue (Onicescu et al., 1999).

The parameters considered for the stress change computation are given in Table 3, while the stress change maps are presented in Fig. 2. The calculation procedure is described analytically in the Appendix A. The main results include: (a) the normal stress acting across the optimal plane for failure (hypocentral region) was reduced by 0.36 bar (unclamping; see Eq. A10 in Appendix) and (b) the Coulomb stress was found positive between 0.51 and 0.78 bar (depending on the effective coefficient of friction – Table 4 and Fig. 3). Unclamping the optimal plane for failure would have locally lowered the resistance to sliding. Such an effect could have been enhanced if the lowered normal stress permitted fluid infusion into the undamped part of the fault (e.g. Perfettini et al., 1999). We also modelled the effect of pore fluid pressure inside the fault zone only to confirm the triggering hypothesis (see Table 6). In our models we accept that negative friction

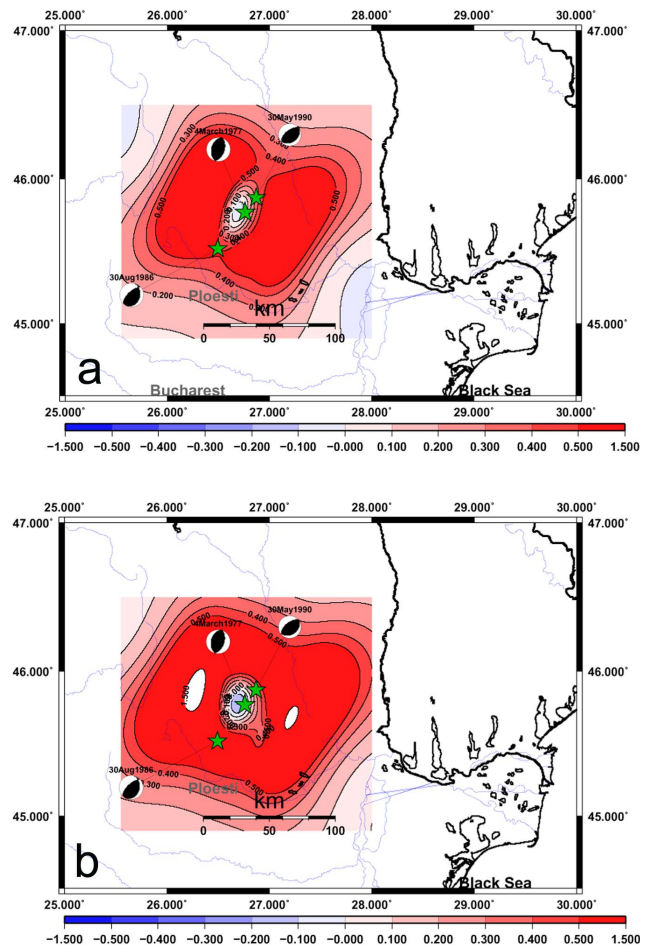


Fig. 2. Map of Coulomb stress due to the 1977 earthquake for optimally oriented faults to regional compression (N307° E) at the depth of 131 km (hypocentral depth of the 1986 event) in the case of (a) effective friction 0.4 and (b) 1. Colour palette of stress values is linear in the range of –0.5 to +0.5 bar (1 bar = 100 kPa). White colour indicates area where transferred stress > 1.5 bar. Green stars show the earthquake epicentres.

values imply pore fluid pressure inside the fault. So accounting for pore pressure change (ΔP , Table 6, lines 3 and 6) we found again that Coulomb stress is increased.

Table 4. Parameters of statistical analysis of Δ CFF for optimal planes at depth 131 km, hypocentre area of 1986 event (40 400 grid points). We can see that by increasing the coefficient of friction, Δ CFF is increased. For a graph view of the results see Fig. 3. For details of the method see Appendix A.

Parameter	$\mu' = 0.4$	$\mu' = 1$
Mean value of Δ CFF	0.31 bar	0.45 bar
Standard Deviation of Δ CFF	0.27 bar	0.35 bar
Minimum of Δ CFF	-0.07 bar	-0.20 bar
Maximum of Δ CFF	1.35 bar	1.69 bar
Range of Δ CFF	1.42 bar	1.89 bar
Δ CFF at 1986 hypocentre	0.51 bar	0.78 bar

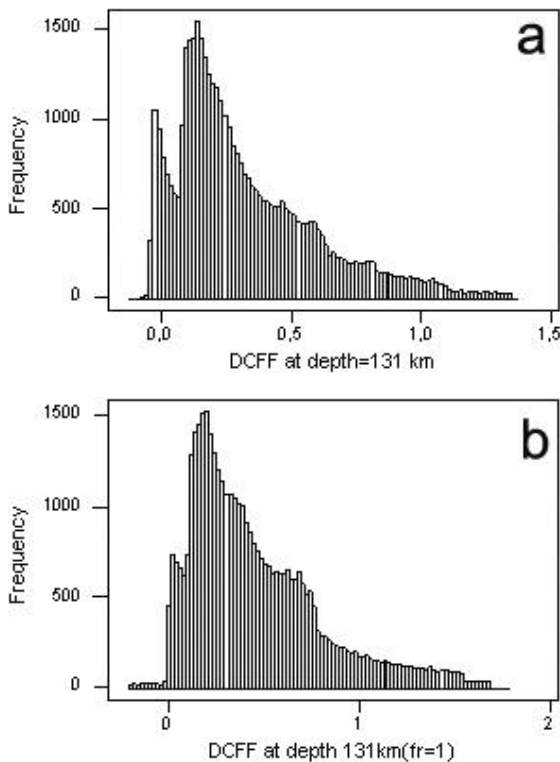


Fig. 3. Histogram of Coulomb stress values at 131 km depth (grid shown in Fig. 2) for effective friction coefficient equal to 0.4 (a) and 1 (b), respectively. It is seen that in (b) histogram values are shifted to the right (i.e. greater) along the x-axis (stress values).

2.2 Triggering of the 1990 earthquake: combination of the 1977 and 1986 earthquakes at depth 89 km

The next step is to evaluate if the combined stress change due to events of 1977 and 1986 can trigger the subsequent event of 1990. We computed Coulomb stress change, on optimally oriented planes, at depth of 1990 hypocenter, 89 km. The target planes are oriented NE-SW, such as the 1990 fault plane (Table 1). Δ CFF was sampled on a horizontal section at 89 km, on a 200 × 200 km grid, with 1 km grid spacing.

Table 5. Parameters of statistical analysis of combined Δ CFF at depth 89 km, hypocentre area of 1990 event (40 400 values) assuming azimuth of tectonic stress at N307° E. We can see that by increasing the coefficient of friction, Δ CFF is increased.

Parameter	$\mu' = 0.4$	$\mu' = 1$
Mean value of Δ CFF	0.40 bar	1.31 bar
Standard Deviation of Δ CFF	4.14 bar	6.06 bar
Minimum of Δ CFF	-60.01 bar	-30.34 bar
Maximum of Δ CFF	368.33 bar	478.81 bar
Range of Δ CFF	428.35 bar	509.16 bar
Δ CFF at 1990 hypocentre	-8.58 bar	-1.05 bar

Table 6. A comparison of Coulomb stress (Δ CFF) values at the 1986 hypocentre (45.52° N, 26.49° E) provided by different triggering algorithms and friction coefficients. Δ CFF is calculated on optimal failure planes at 131 km depth (top three rows), and for 1986-type striking reverse faults at 131 km depth, bottom three rows). Friction coefficients 0.4 and 1 assume that no pore pressure changes exist ($\Delta P = 0$ in Eq. 2). In the case $\mu' = -0.2$, ΔP equals 1.099 bar.

Friction coefficient	$\Delta\sigma_n$ (bar)	$\Delta\tau$ (bar)	Δ CFF (bar)	Algorithm	Figure
0.4	0.365	0.369	0.516	Optimal planes	2a
1	0.499	0.281	0.781	Optimal planes	2b
-0.2*	0.296	0.390	0.669	Optimal planes	
0.4	-0.455	-0.849	-1.031	Rake angle	5a
1	-0.455	-0.849	-1.304	Rake angle	5b
-0.2*	-0.455	-0.849	-0.720	Rake angle	

* incl. pore fluids.

For 1986 earthquake of magnitude $M_w = 7.1$, following relations (5) and (6), we estimated a strike-slip displacement of -0.1423 m, and a dip-slip displacement of -0.5708 m. The displacements were calculated by using Eq. (3) for the relation $M_o - M_w$. For the 1986 rupture we assumed a length of 40 km and a width of 30 km (rupture area 1200 km²), respectively.

Our results (Fig. 4a and b) indicate that the hypocentre of the 1990 event is located inside the relaxed area of the combined static stress field. However, the location of the hypocentre is close to the boundary between relaxed and loaded Coulomb stress lobes, which indicates that the solution is sensitive to the slip model used for the 1977 event. The 1977 event is larger ($M = 7.4$) than 1986 ($M = 7.1$) and its hypocentre is closer to the 1990 hypocentre. So the static stress changes at depths around 90 km are dominated by the 1977 slip model. In fact, in the case of effective friction coefficient = 1 the 1990 epicentre is located about 2 km to the west of the boundary of the positive, combined lobe. Also the amount of the Coulomb stress (relaxation) is reduced from -8.58 bar to -1.05 bar, or by a factor of 8 (Table 5).

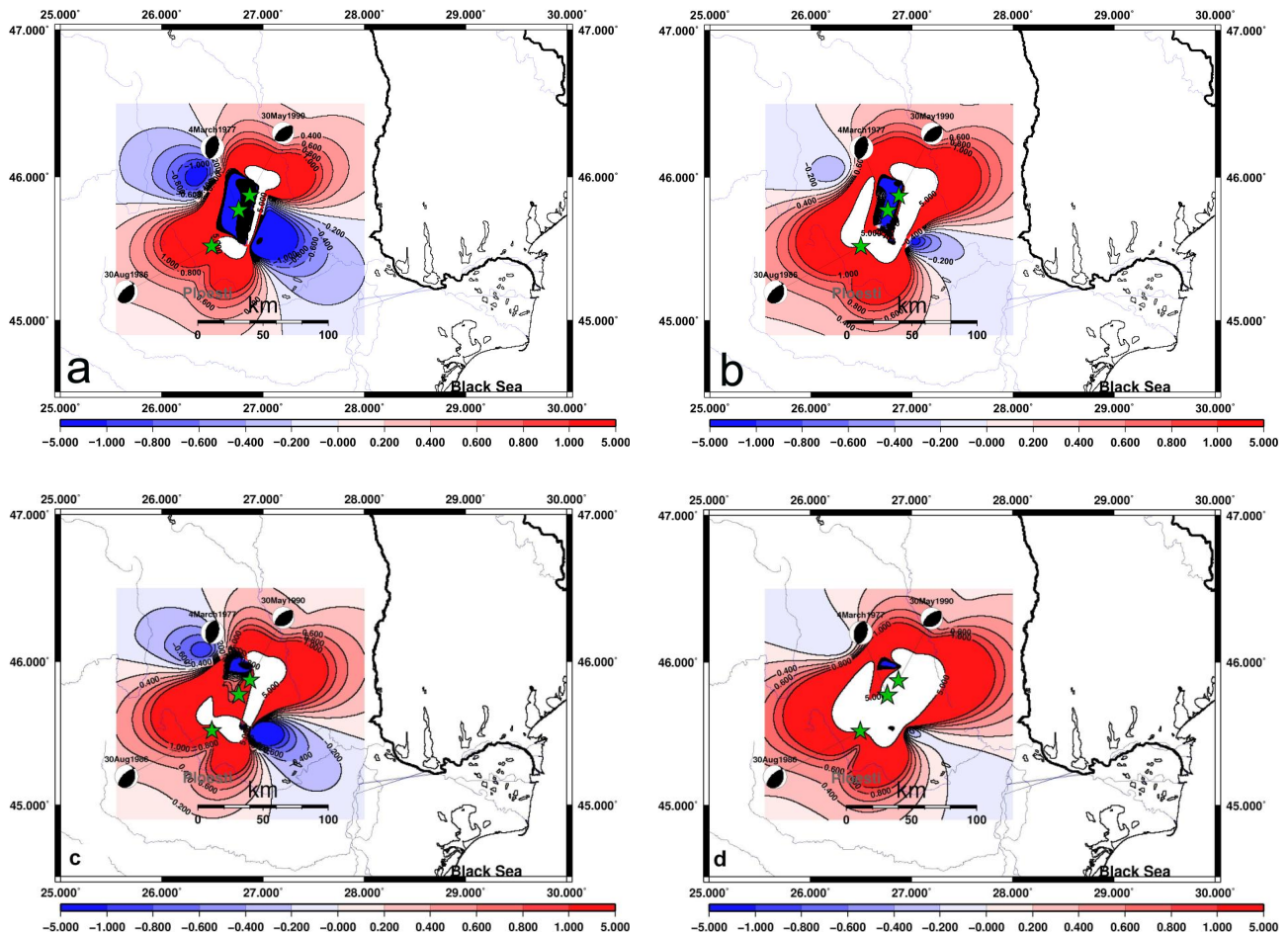


Fig. 4. Maps of combined ΔCFF for the 1977 and 1986 earthquakes for optimally oriented faults to regional compression ($\text{N}307^\circ\text{E}$) at depth of 89 km (hypocentral depth of 1990 event). (a) Friction $\mu' = 0.4$. (b) Friction $\mu' = 1$. Colour palette of stress values is linear in the range of -1 to $+1$ bar (1 bar = 100 kPa). Blue areas indicate unloading, red areas indicate loading, respectively. White colour indicates area where transferred stress > 5 bar and black colour the area where stress reduction was < -5 bar. Green stars show the earthquake epicentres. (c) Map of combined ΔCFF for regional compression $\text{N}323^\circ\text{E}$ and $\mu' = 0.4$. (d) Map of combined ΔCFF for regional compression $\text{N}323^\circ\text{E}$ and $\mu' = 1$.

We repeated the Coulomb stress calculations using a different azimuth for the regional stress field, namely $\text{N}323^\circ\text{E}$ which was provided by the fault plane solution of the 1990 event (see Table 2; computed by the RAKE program; Louvari and Kiratzi, 1997). In Fig. 4c and d, optimally oriented faults to regional compression ($\text{N}323^\circ\text{E}$), which is principal P-axis azimuth of the 1990 event, is assumed. Using this scenario we arrive at the opposite conclusion, i.e. that the 1990 earthquake was triggered by the combined field of the 1977 and 1986 events. The values obtained at the 1990 hypocenter are (Table 7, cases 7 and 8) 2.70 bar for apparent friction = 0.4 and 13.76 bar for apparent friction = 1, respectively. We highlight the sensitivity of our results to the azimuth of the regional stress field as the difference is only 16° .

Table 7. Values of Coulomb stress at the 1990 hypocentre (45.87°N , 26.87°E , 89 km) for optimally oriented planes to regional compression (cases 1 to 3) and for 1990-type target planes (cases 4 to 6), respectively. Cases 7 and 8 show ΔCFF values assuming a regional compression azimuth of $\text{N}323^\circ\text{E}$.

Case	Friction coefficient	ΔCFF (bar)	Algorithm	Figure
1	0.4	8.57	Optimal planes – $\text{N}307^\circ\text{E}$	4a
2	1	-1.05	Optimal planes – $\text{N}307^\circ\text{E}$	4b
3	-0.2*	-12.05	Optimal planes – $\text{N}307^\circ\text{E}$	
4	0.4	-23.75	Rake angle	
5	1	-15.68	Rake angle	
6	-0.2*	-26.22	Rake angle	
7	0.4	2.70	Optimal planes – $\text{N}323^\circ\text{E}$	4c
8	1	13.76	Optimal planes – $\text{N}323^\circ\text{E}$	4d

* incl. pore fluids.

3 Discussion

3.1 Stress changes on the reactivated faults

Our computations start from the hypothesis of an oceanic-type lithosphere for the subducted slab. This is largely adopted by many researchers, but there are also opinions in favor of a continental delaminated lithosphere in Vrancea (e.g. Knapp et al., 2005; Koulakov et al., 2010). For the purposes of this study the difference concerns the mechanical properties of the deforming material (i.e. Poisson ratio and shear modulus), as earthquakes are modeled as due to shear failure. Assuming elastic rheology and Coulomb-type failure for an oceanic lithosphere setting we propose that the earthquake triggering is possible for Vrancea given realistic effective coefficient of friction values (0.1–1).

In Sect. 2.1 we calculated stress changes throughout the upper mantle for optimal planes of failure using the *strop* algorithm. The dip-angle θ of such planes would be $22 < \theta < 42^\circ$ for effective coefficient of friction values (0.1–1). Notice that the dips of both NW-dipping, 1986 and 1990, faults are within the range of dip-angles 56° – 68° (see Table 1 for fault plane attributes; $\theta = 41^\circ$ for the 1977 event), or high-angle faults. We interpret this high-angle orientation as result of rotation of faults with progressive strain of the slab relative to a horizontal rotation axis. Rotation of faults is necessary to accommodate deformation of the slab in both directions (assuming plane strain): vertical elongation and horizontal shortening.

As a variation, Δ CFF can be calculated on planes of fixed orientation if it is known that there is a fabric of existing thrust faults in Vrancea which are likely to provide planes of failure. In such case we investigate Coulomb stress along specified fault planes, not planes optimally oriented to regional compression. Such planes (if existing) can host earthquake ruptures. We assume that NE-SW striking, northwest dipping reverse faults in the Vrancea area will be of interest as candidates for failure. First we examine the triggering scenario of the 1986 earthquake. We use *strop* (stress_on_planes) in this run to calculate Δ CFF on planes of specified orientation identical to the 1986 event (Table 1) at 131 km depth (the 1986 hypocentre depth; Fig. 5). We found that triggering is discouraged as the Δ CFF values are negative for all effective coefficients of friction considered (Table 6). We also took into account pore fluid pressure effects (negative effective coefficient of friction) and found both similar Δ CFF patterns and values (Table 6; $\mu' = -0.2$). This opposite result to the optimal planes (*strop*) model would require more seismological data to investigate, such as the slip distribution of the 1977 rupture (which is not available to us). This result leaves the case open for future investigation as to if the 1986 earthquake in Vrancea was promoted by the 1977 event.

The same modeling procedure was followed in the case of the 1990 event, where stress transfer due to combined slip models of 1977 and 1986 was calculated on 1990-type fault

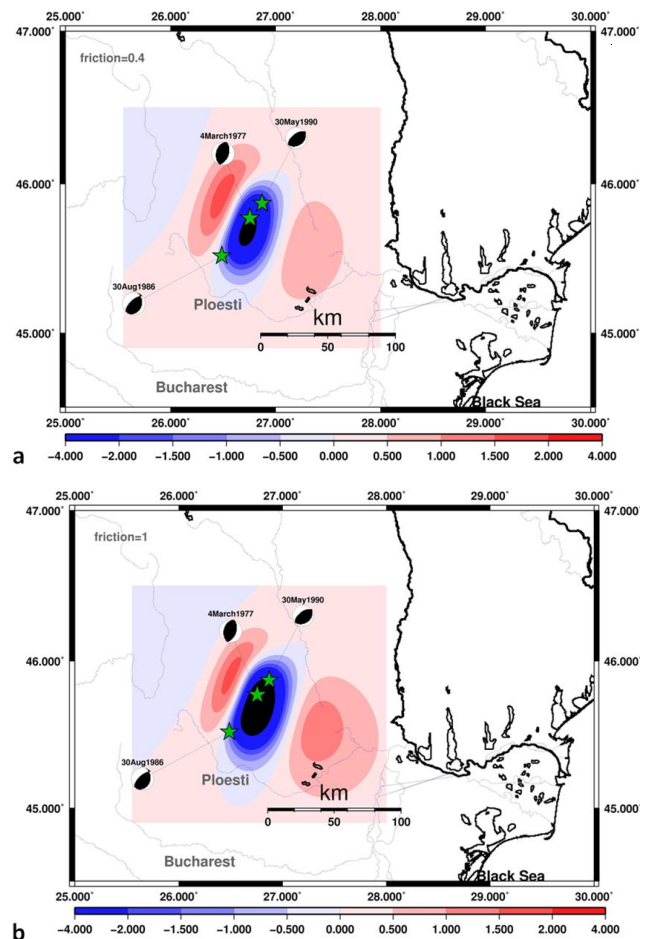


Fig. 5. Map of Coulomb stress due to the 1977 earthquake for 1986-type receiver faults at the depth of 131 km (hypocentral depth of the 1986 event) in the case of (a) effective friction 0.4 and (b) 1. Colour palette of stress values is linear in the range of -4 to $+4$ bar (1 bar = 100 kPa). Black colour indicates area where transferred stress < -4 bar. Green stars show the earthquake epicenters.

planes (Table 7 lines 4, 5 and 6). We also find no triggering relation for this event as Δ CFF values at the 1990 hypocentre range from -15 to almost -26 bar.

Therefore, it is suggested that a triggering relationship is possible between the 1977 and 1986 events as the optimal planes stress transfer model results in loading of the 1986 hypocentre. A similar result is obtained for the 1990 earthquake if we assume that the compression direction is $N323^\circ E$. However, modeling the 1990 event using the rake angle (fault specific) model and homogeneous slip shows that its occurrence is not related to Coulomb stress transfer from the two previous earthquakes. We found that the 1990 hypocentre is located in the stress shadow of the combined 1977 and 1986 stress field. We note that the entire fault (hosted the 1990 event) is not expected to lie inside the shadow because of its large dimensions (rupture width probably 30 km or more according to the empirical relationships

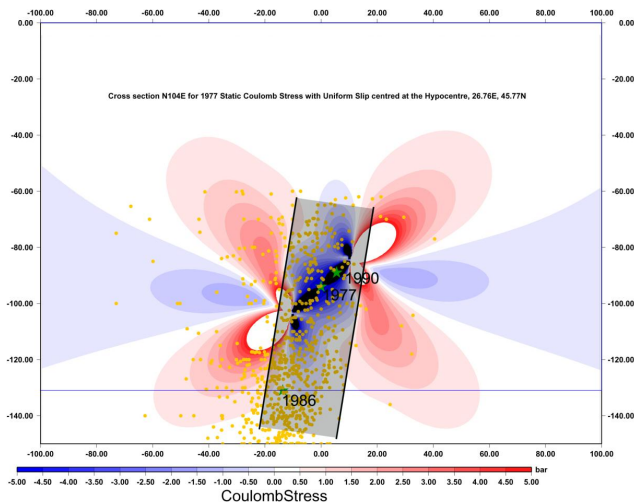


Fig. 6. Cross section of the Coulomb stress field due to 1977 earthquake (depth = 94 km assuming an effective friction of 0.4). Strike of section is N104° E. Section centre point is the 1977 hypocentre. Colour palette of stress values is linear in the range of -5 to $+5$ bar (1 bar = 100 kPa). Blue areas indicate unloading, red areas indicate loading, respectively. White colour indicates area where transferred stress > 5 bar and black colour the area where stress reduction was < -5 bar. Green stars show the earthquake hypocentres. Blue line at 131 km depth shows the map view of Fig. 2a. Solid yellow circles are aftershocks (1977–1986). Shaded rectangle indicates shape of Vrancea slab (dip to the West).

of Wells and Coppersmith, 1994). In this interpretation, the 1990 earthquake was, most probably, due to shear failure of an unbroken patch of the 1977 fault. Note that the 1990 hypocentre is located about 15 km to the NE of the 1977 one and towards up-dip.

3.2 Aftershock distribution

In order to visualize the spatial correlation of stress transfer lobes along the slab (down-dip dimension) with the distribution of off-fault aftershocks we constructed vertical cross sections (Figs. 6 and 7). The stress changes have been calculated throughout the upper mantle for optimal planes of failure using the *stroop* algorithm. We observe that most 1977 aftershocks (82%) occurred inside loaded areas of the slab (planes optimally oriented to failure) and to the down-dip direction (Fig. 6). The aftershocks are occupying mostly a vertical volume of material and occur at distances as much as 50 km from the hypocenter (Fig. 6; we consider the distance in the E-W horizontal direction). A small E-W spreading of aftershocks with depth is observed, as well. It is possible that the slab spreads horizontally as it descends into the asthenosphere, thus providing enough elasticity for rupture. Also, there is seismic tomography evidence (Wenzel et al., 2002) for a systematic spreading of the high-velocity body with depth.

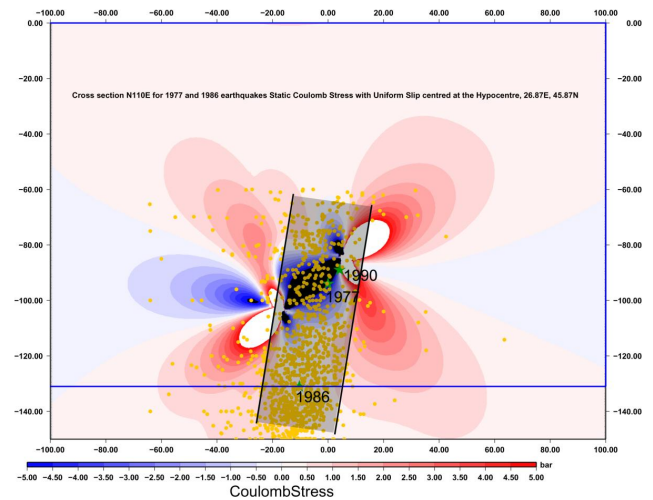


Fig. 7. Cross section of the combined Coulomb stress field due to 1977 and 1986 earthquakes (assuming an effective friction of 0.4). Strike of section is N110° E. Section centre point is the 1990 hypocentre. Colour palette of stress values is linear in the range of -5 to $+5$ bar (1 bar = 100 kPa). Blue areas indicate unloading, red areas indicate loading, respectively. White colour indicates area where transferred stress > 5 bar and black colour the area where stress reduction was < -5 bar. Green stars show the earthquake hypocentres. Solid yellow circles are aftershocks (1977–1990). Shaded rectangle indicates shape of Vrancea slab (dip to the West).

Aftershocks occurring inside the relaxed area (along dip the Vrancea slab) are not explained by our homogeneous slip model but could be due to (a) heterogeneous slip that modifies the static stress transfer change across the fault, (b) on damage in the vicinity of the rupture (brittle microcracking), and (c) transmitted dynamic stress changes.

3.3 Implications for slab tectonics and large earthquakes

Given that intermediate-depth seismicity in Vrancea is clustered (Purcaru, 1979; Byrdina et al., 2006; Huruikawa et al., 2008) there may be some basis for putting forward arguments for recurrence of strong earthquake activity based on the stress transfer results. We show a seismicity map in Fig. 8 with all intermediate-depth events with $M_w > 4.8$ as provided by the Global CMT database (<http://www.globalcmt.org/>). There are 19 events in this catalogue spanning a period of 33 years (1976–2010; Table 8). The map shows a NE-SW arrangement of epicentres, about 70–80 km long, all but one of which represented by reverse faulting mechanisms. The range of hypocentral depths is 83–154 km. When projected on a ESE-WNW cross-section (Fig. 9) it is seen that there are two clusters, an upper-plate (90 ± 10 km) cluster and a lower-plate (130 ± 10 km). A similar result was obtained by analysis of Romanian earthquake data by Rogozea et al. (2009). The majority of the projected mechanisms

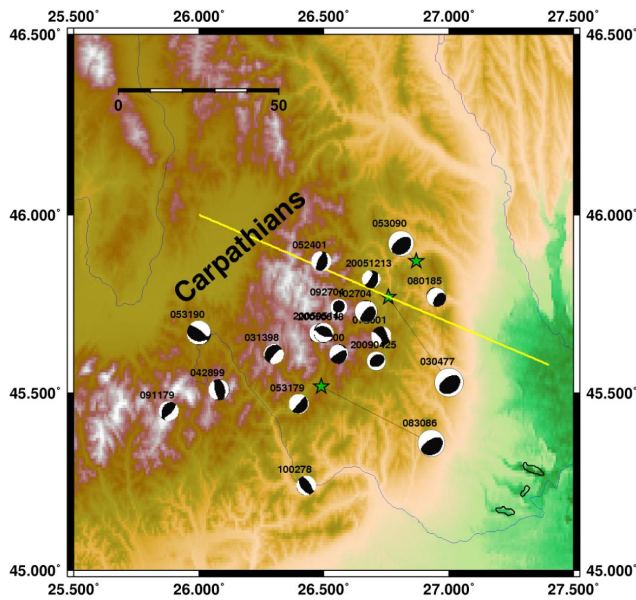


Fig. 8. Map of south Carpathian region (Romania) showing focal mechanisms of intermediate-depth earthquakes from the global CMT database using a lower-hemisphere stereographic projection. The date of each event is written above each sphere. Black colour indicates compressional quadrant. The fault plane responsible for each earthquake will be parallel to one of the nodal planes. Green stars are epicenters of the 1977, 1986 and 1990 earthquakes. Yellow line shows the vertical cross-section of Fig. 8 (the line passes through the 1977 epicentre which is the first event of the sequence that we investigate in this paper). The line is 104 km long and the azimuth is N117° E.

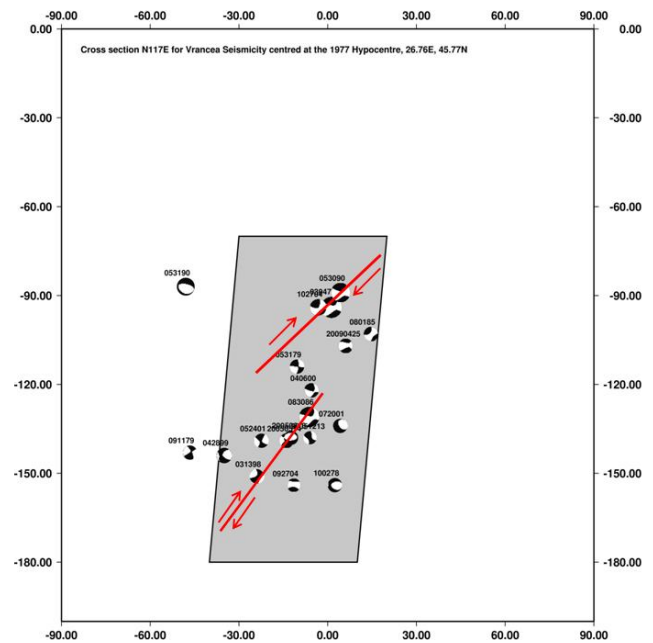


Fig. 9. Cross-section of intermediate-depth seismicity reported at Table 8, oriented ESE-WNW. Beach balls represent the frontal projections of the available fault plane solutions of Fig. 8, in order to indicate the kinematics of the deformation. The date of each event is written above each sphere. Shaded rectangle shows the possible extent of the dipping slab. Red lines indicate location of major faults.

of the same earthquake population (Fig. 9) indicate down-dip extension along mainly west-dipping planes (Fig. 10). This geometrical arrangement, combined with the similarity in kinematics (thrust type of most earthquake motions in combination with slab extension along dip), points to a possible pattern of two, major planes of weakness along the slab separated by a distance of 30 ± 10 km (we mean vertical distance, i.e. down-dip, between the proposed fault planes). We acknowledge that the proposed clustering may not be so evident given the errors in CMT hypocentral determinations. However, we advocate a tectonic model which is constrained by the 3 strongest events (1977, $M = 7.4$; 1986, $M = 7.1$ and 1990, $M = 6.9$) assuming that they occurred on the main fault planes (planes of weakness) inside the Vrancea slab. However, a possible third, parallel plane of weakness, further deeper (at 160 km depth) cannot be excluded. Such a plane is possible to release the strain energy stored at the 160 km depth, considered a seismic gap by Hurukawa et al. (2008). We note that a depth of 150 km has been proposed by Oncescu et al. (1997) for the greatest (so far) event of Vrancea (10 November 1940).

Table 8. List of intermediate depth events with $M > 4.8$ for the period 1976–2010 (source Global CMT Catalog, <http://www.globalcmt.org>). ** indicates depth after Oncescu and Bonjer, 1997. * indicates optimal orientation to compression axis (N307° E–N323° E, $\pm 10^\circ$). 10 out of 19 events are included in that range. Strike/Dip/Rake angles are in degrees.

	Event	Magnitude	Depth (km)	Strike	Dip	Rake
1*	4 Mar 1977	7.5	83/94**	194	41	87
2	2 Oct 1978	5.1	154	326	51	94
3*	31 May 1979	5.2	114	221	85	92
4	11 Sep 1979	5.1	142	202	29	70
5	1 Aug 1985	5.2	102	288	9	-14
6*	30 Aug 1986	7.2	132/131**	227	65	104
7*	30 May 1990	6.9	74/89**	232	58	89
8	31 May 1990	6.3	87	309	69	106
9*	13 Mar 1998	5.2	151	227	12	96
10	28 Apr 1999	5.4	143	166	54	88
11*	6 Apr 2000	5.1	122	238	81	106
12*	24 May 2001	5.2	139	208	60	104
13	20 Jul 2001	5.2	133	119	77	44
14	27 Sep 2004	4.8	154	198	40	75
15*	27 Oct 2004	5.8	93	219	81	107
16	14 May 2005	5.2	139	183	50	71
17	18 Jun 2005	5.0	138	293	32	90
18*	13 Dec 2005	4.8	138	219	76	112
19*	25 Apr 2009	5.2	106	230	46	77

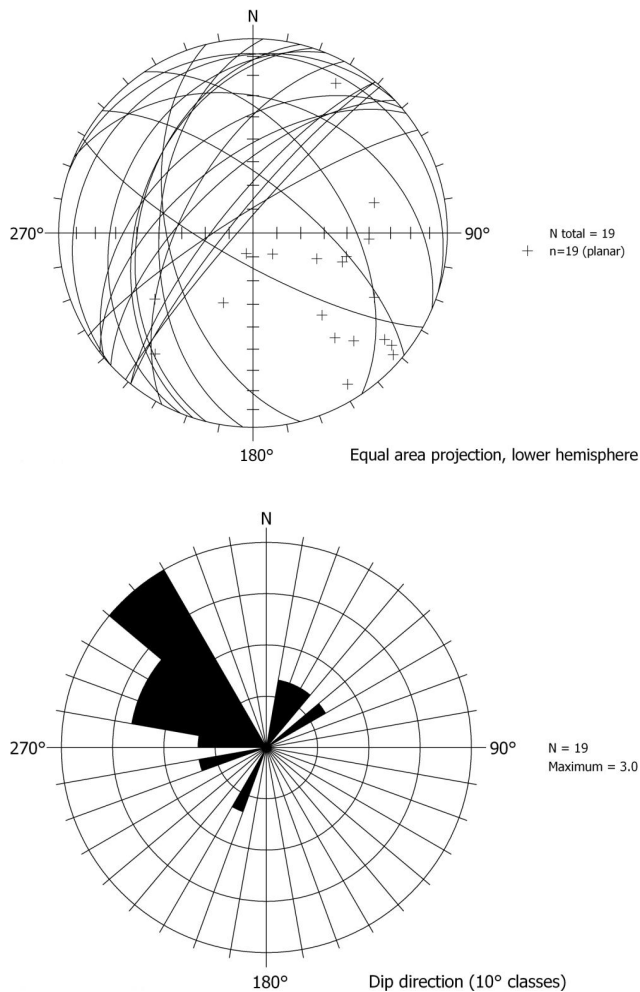


Fig. 10. Equal-area, lower hemisphere projection (top) of fault plane projections of intermediate depth events and rose-diagram of dip directions (bottom). Fault planes are shown as great circles and dip predominantly to the NW. Data is shown in Table 8.

Our stress transfer results show that enough Coulomb stress is transferred at distances over 30–40 km down-dip and/or up-dip the Vrancea slab to trigger a large earthquake along optimally oriented fault planes to regional compression (such as planes of weakness inside the slab). Moreover, the stress shadow effect is cumulative with time (see location of relaxed lobes – zones in Figs. 6 and 7; Harris and Simpson, 1998), as the thrust-type kinematics of the deformation do not change. This results in repeated loading of the areas both up-dip and down-dip of the fault but also, in repeated unloading of the areas above and below the fault (see section in Fig. 6 for geometry and Coulomb stress distribution) assuming homogeneous slip distribution and elastic (Okada) rheology. Following this, we suggest that there is no significant tectonic stress to be accumulated at depths below 90 km and above 130 km (± 10 km for both depths). Any earthquakes to occur at this depth interval are most likely to be

moderate events ($M < 6$; Fig. 9). If this triggering scenario is valid, then the two NW-dipping planes (pictured in Fig. 9) are efficient to transmit and receive Coulomb stresses from successive earthquake ruptures, thus releasing the accumulated strain seismically and displaying a clustering pattern in space and time. This setting resembles the stress feedback mechanism that drives fault growth inside rift systems (Cowie, 1998).

4 Conclusions

We found that earthquake triggering by static stress transfer can occur at intermediate seismogenic depths (90–131 km) as demonstrated in the case of the 1986 event in the Vrancea region, Romania. Our computations start from the hypothesis of an oceanic-type lithosphere for the subducted slab (e.g. Tondi et al., 2009). Using elastic rheology we propose that for Vrancea-type slabs earthquake triggering can occur given a wide range of coefficient of friction values (0.1–1), including pore fluid pressure effects along the fault plane.

Our results show that:

1. The 1986 event may have been triggered by static stress transfer because it occurred along a reverse fault plane with similar kinematics to the 1977 earthquake. This earthquake occurred 40 km down-dip the slab and 30 km to the SW of the 1977 hypocentre. The 1986 hypocentre is found inside a loaded stress lobe in the case of optimally oriented planes to the regional compression. However, modeling stress transfer along 1986-type (specific) receiver faults did not show triggering.
2. Despite its proximity to the 1977 hypocentre, it is uncertain if the 1990 earthquake was triggered by static stress transfer as the results for target faults oriented optimally to the regional stress field are highly sensitive to the azimuth of the maximum compression (N307° E vs. N323° E).
3. Using the (NW-dipping) slip model of the 1990 event as the receiver fault of the combined 1977 and 1986 static stress fields, the former hypocentre lies inside a relaxed (unloaded) area of the slab. In that case the 1990 event most likely represents an unbroken patch (asperity) of the 1977 rupture plane (Fig. 9, upper part) that failed due to long-term loading.
4. Large earthquakes ($M > 6.8$) in Vrancea are clustered at the depths of 90 and 130 km possibly because of the existence of two, major planes of weakness (faults) that are located at “triggerable” distances (one fault length) down-dip the slab (Fig. 9). The two faults accommodate the deformation of the slab (down-dip extension) by shear failure. Their high-angles relative to the shortening axis is due to rotation towards the elongation direction with progressive strain. A third, sub-parallel, major, NW-dipping plane of weakness at depth of 160 km cannot be excluded.

Appendix A

Calculation of ΔCFF for optimal planes. Equations after Jaeger and Cook (1979), p. 13 (Fig. 2 in the text)

First, we compute the regional (tectonic) stress field as follows.

Assuming uniaxial compression (*negative convention*; σ_t) the value of the maximum horizontal stress σ'_x is

$$\sigma'_x = \left[\sigma_x \cdot \cos^2(az) \right] + \left[\sigma_y \cdot \sin^2(az) \right] \quad (A1)$$

where $az = 307^\circ$ and $\sigma_x = 0$, and $\sigma_y = \sigma_t = -500$ bar, so $\sigma'_x = -318.9$ bar and the value of the minimum horizontal stress σ_y is given by

$$\sigma'_y(\text{bar}) = \text{sig } x \cdot \sin^2(az) + \text{sig } y \cdot \cos^2(az) \quad (A2)$$

where $az = 307^\circ$ and $\sigma_x = 0$, so $\sigma'_y = -181.09$ bar and the value of the shear stress τ_{xy} is given by

$$\tau'_{xy} = 0.5 \cdot (\sigma_y - \sigma_x) \cdot \sin(2az) \quad (A3)$$

where $az = 307^\circ$ and $\sigma_x = 0$, so $\tau'_{xy} = 240.31$ bar

Assuming no lithostatic stress field the values of $\sigma'_x \sigma'_y$ and τ'_{xy} are the same for the ambient stress field components s_{11} , s_{22} and s_{12} , respectively.

Taking $s_{33} = 0$, $s_{13} = 0$ and $s_{23} = 0$ we solve for the eigenvalues (principal stresses of the ambient field) of the equation (Jaeger and Cook, 1979, p. 20):

$$\begin{vmatrix} s_{11} - \sum & s_{12} & s_{13} \\ s_{21} & s_{22} - \sum & s_{23} \\ s_{31} & s_{32} & s_{33} - \sum \end{vmatrix} = 0$$

where $s_{11} = (A1)$, $s_{22} = (A2)$, $s_{33} = 0$, and $s_{12} = (A3)$

$$\begin{matrix} S_{\min}(\text{bar}) & S_{\text{int}}(\text{bar}) & S_{\max}(\text{bar}) \\ -499.9999999944 & 0 & 0.000000005574 \end{matrix} \quad (A4)$$

Then, we compute the total stress field as follows:

$$\sigma_{ij}(\text{total}) = \sigma_{ij}(\text{initial}) + \sigma_{ij}(\text{ambient}) \quad (A5)$$

where $\sigma_{ij}(\text{initial})$ is the output of the ELFGRID algorithm, and $\sigma_{ij}(\text{ambient})$ is given by (A1, A2 and A3)

Solution A4 is combined.

Then we solve for the eigenvalues of Eq. (A5) using

$$\left| \sigma_{ij}(\text{total}) - \sum = 0 \right|$$

and we obtain the following principal stresses of the total field

$$\begin{matrix} S_{\min}(\text{bar}) & S_{\text{int}}(\text{bar}) & S_{\max}(\text{bar}) \\ -500.18045000 & -3.73492742 & 0.61631757 \end{matrix} \quad (A6)$$

Then, we compute the change in normal stress $\Delta\sigma_n$ acting on the optimal plane as follows.

First we compute the normal stress for the total field (using values from A6):

$$\begin{aligned} \sigma(\text{total}) &= (1/2) \cdot (\sigma_1 + \sigma_3) + (1/2) \cdot (\sigma_1 - \sigma_3) \cos 2\beta \\ &- 156.78644110 \end{aligned} \quad (A7)$$

where

$$\cos 2\beta = -\mu \cdot (\mu^2 + 1)^{-1/2} \quad (A8)$$

and μ is the coefficient of apparent friction.

Then we compute the normal stress for the ambient field (using values from A4):

$$\begin{aligned} \sigma(\text{amb}) &= (1/2) \cdot (\sigma_1 \text{amb} + \sigma_3 \text{amb}) \\ &+ (1/2) \cdot (\sigma_1 \text{amb} - \sigma_3 \text{amb}) \cos 2\beta \\ &- 157.15233091 \end{aligned} \quad (A9)$$

and $\cos 2\beta$ same as in (A8).

So, the change in normal stress is given by (A7)–(A9)

$$\begin{aligned} \Delta\sigma_n &= \sigma(\text{total}) - \sigma(\text{ambient}) \\ &0.36588980 \text{ bar} \end{aligned} \quad (A10)$$

Similarly, we compute the change in shear stress $\Delta\tau$ acting along the optimal plane as follows:

$$\begin{aligned} \tau(\text{total}) &= (-1/2) \cdot (\sigma_1 - \sigma_3) \sin 2\beta \\ &232.48906278 \end{aligned}$$

$$\begin{aligned} \tau(\text{ambient}) &= (-1/2) \cdot (\sigma_1 \text{amb} - \sigma_3 \text{amb}) \sin 2\beta \\ &232.11917272 \text{ bar} \end{aligned}$$

$$\begin{aligned} \Delta\tau &= \tau(\text{total}) - \tau(\text{ambient}) \\ &0.36989006 \text{ bar} \end{aligned} \quad (A11)$$

where

$$\sin 2\beta = (\mu^2 + 1)^{-1/2} \quad (A12)$$

Therefore, the Coulomb stress is after (A11) and (A10) above:

$$\begin{aligned} \Delta\text{CFF} &= \Delta\tau + \mu' \Delta\sigma_n \\ &0.51624598 \text{ bar} \end{aligned}$$

Or the value in Table 4.

Acknowledgements. We thank NATO Science for Peace Project 981881 for financing the stay of Bogdan Grecu to Athens where this modeling was done. We thank Ritsa Papadimitriou and Chung-Han Chan for constructive reviews. We are indebted to George Drakatos, Tom Parsons, Andrei Bala and Kostas Makropoulos for discussions. We acknowledge Bob Simpson for making available the DLC code and Mary Kolligri for help with focal parameter calculations. All illustrations were prepared using the GMT software except for Figure 10 which was prepared using the software STEREO32.

Edited by: M. E. Contadakis

Reviewed by: E. Papadimitriou and C.-H. Chan

References

- Byrdina, S., Shebalin, P., Narteau, C., and Le Mouél, J. L.: Temporal properties of seismicity and largest earthquakes in SE Carpathians, *Nonlin. Processes Geophys.*, 13, 629–639, doi:10.5194/npg-13-629-2006, 2006.
- Cowie, P. A.: A healing-reloading feedback control on the growth rate of seismogenic faults, *J. Struct. Geol.*, 20, 1075–1087, 1998.
- Fan, G., Wallace, T. C., and Zhao, D.: Tomographic imaging of deep velocity structure beneath the Eastern and Southern Carpathians, Romania: implications for continental collision, *J. Geophys. Res.*, 103(B2), 2701–2723, 1998.
- Freed, A. M.: Earthquake triggering by static, dynamic, and post-seismic stress transfer, *Annu. Rev. Earth Pl. Sc.*, 33, p. 335, doi:10.1146/annurev.earth.33.092203.122505, 2005.
- Ganas, A., Shanov, S., Drakatos, G., Dobrev, N., Sboras, S., Tsimi, C., Frangov, G., and Pavlides, S.: Active fault segmentation in southwest Bulgaria and Coulomb stress triggering of the 1904 earthquake sequence, *J. Geodyn.*, 40, 316–333, 2005.
- Ganas, A., Gosar, A., and Drakatos, G.: Static stress changes due to the 1998 and 2004 Krn Mountain (Slovenia) earthquakes and implications for future seismicity, *Nat. Hazards Earth Syst. Sci.*, 8, 59–66, doi:10.5194/nhess-8-59-2008, 2008.
- Gomberg, J., Reasenber, P. A., Bodin, P., and Harris, R. A.: Earthquake triggering by seismic waves following the Landers and Hector mine earthquakes, *Nature*, 411, 462–466, 2001.
- Hanks, T. C. and Kanamori, H.: A moment magnitude scale, *J. Geophys. Res.*, 84, 2348–2350, 1979.
- Harris, R. A. and Simpson, R. W.: Suppression of large earthquakes by stress shadows: A comparison of Coulomb and rate and state failure, *J. Geophys. Res.*, 103, 439–451, 1998.
- Harris, R. A., Simpson, R. W., and Reasenber, P. A.: Influence of static stress changes on earthquake locations in southern California, *Nature*, 375, 221–224, 1995.
- Hurukawa, N., Popa, M., and Radulian, M.: Relocation of large intermediate-depth earthquakes in the Vrancea region, Romania, since 1934 and a seismic gap, *Earth Planets Space*, 60, 565–572, 2008.
- Imoto, M. and Hurukawa, N.: Assessing potential seismic activity in Vrancea, Romania, using a stress-release model, *Earth Planets Space*, 58, 1511–1514, 2006.
- Ismail-Zadeh, A. T., Panza, G. F., and Naimark, B. M.: Stress in the descending relic slab beneath Vrancea, Romania, *Pure Appl. Geophys.*, 157, 111–130, 2000.
- Jaeger, J. C. and Cook, N. G. W.: *Fundamentals of Rock Mechanics*, 3rd edn., Chapman and Hall, London, UK, 13–20, 1979.
- Kiratzis, A.: Active deformation in the Vrancea region, Rumania, *Pure Appl. Geophys.*, 140, 391–402, 1993.
- Knapp, J. H., Knapp, C. C., Raileanu, V., Matenco, L., Mocanu, V., and Dinu, C.: Crustal constraints on the origin of mantle seismicity in the Vrancea Zone, Romania: The case for active continental lithospheric delamination, *Tectonophysics*, 410(1–4), 311–323, doi:10.1016/j.tecto.2005.02.020, 2005.
- Koch, M.: Nonlinear inversion of local seismic travel times for the simultaneous determination of the 3D-velocity structure and hypocentres – application to the seismic zone Vrancea, *J. Geophys.*, 56, 160–173, 1985.
- Koulakov, I., Zaharia, B., Enescu, B., Radulian, M., Popa, M., Parolai, S., and Zschau, J.: Delamination or slab detachment beneath Vrancea? New arguments from local earthquake tomography, *Geochem. Geophys. Geosy.*, 11, Q03002, doi:10.1029/2009GC002811, 2010.
- Ledermann, P. and Heibach, O.: Stress transfer modelling of the strong earthquake sequence at intermediate depths in the Vrancea area, Romania, *GRA*, 9, 02161, SRef-ID:1607-7962/gra/EGU2007-A-02161, 2007.
- Louvari, E. and Kiratzis, A.: Rake: a window's program to plot earthquake focal mechanisms and stress orientation, *Comput. Geosci.*, 23, 851–857, 1997.
- Okada, Y.: Internal deformation due to shear and tensile faults in a half-space, *B. Seismol. Soc. Am.*, 82, 1018–1040, 1992.
- Oncescu, M. C.: Deep structure of Vrancea region, Romania, inferred from simultaneous inversion for hypocenters and 3-D velocity structure, *Ann. Geophys.*, 2, 23–28, 1984.
- Oncescu, M. C.: On the stress tensor in Vrancea region, *J. Geophys.*, 62, 62–65, 1987.
- Oncescu, M. C. and Bonjer, K. P.: A note on the depth recurrence and strain release of large Vrancea earthquakes, *Tectonophysics*, 272, 291–302, 1997.
- Oncescu, M. C., Marza, V. I., Rizescu, M., and Popa, M.: The Romanian Earthquake Catalogue between 984–1997, in: *Vrancea Earthquakes, Tectonics, Hazard and Risk Mitigation*, edited by: Wenzel, F., Lungu, D., and Novak, O., Kluwer Academic Publishers, Dordrecht, Netherlands, 1999.
- Oth, A., Wenzel, F., and Radulian, M.: Source parameters of intermediate-depth Vrancea (Romania) earthquakes from empirical Green's functions modeling, *Tectonophysics*, 438, 33–56, 2007.
- Parsons, T., Yeats, R. S., Yagi, Y., and Hussain, A.: Static stress change from 8 October, 2005 M=7.6 Kashmir earthquake, *Geophys. Res. Lett.*, 33, L06304, doi:10.1029/2005GL025429, 2006.
- Perfettini, H., Stein, R. S., Simpson, R., and Cocco, M.: Stress transfer by the 1988–1989 M=5.3 and 5.4 Lake Elsman foreshocks to the Loma Prieta fault: Unclamping at the site of peak mainshock slip, *J. Geophys. Res.*, 104(B9), 20169–20182, 1999.
- Purcaru, G.: The Vrancea, Romania, earthquake of March 4, 1977 – a quite successful prediction, *Phys. Earth Planet. In.*, 18, 274–287, 1979.
- Radulian, M. and Popa, M.: Scaling of the source parameters for the Vrancea intermediate depth earthquakes, *Tectonophysics*, 261, 67–81, 1996.
- Reasenber, P. A. and Simpson, R. W.: Response of regional seismicity to the static stress change produced by Loma Prieta earthquake, *Science*, 255, 1687–1690, 1992.
- Rogozea, M., Popa, M., and Radulian, M.: Detailed seismicity in the Vrancea area and implications for the seismic cycle evolution, *Rom. Rep. Phys.*, 61, 740–747, 2009.
- Sperner, B., Lorenz, F., Bonjer, K., Hettel, S., Muller, B., and Wenzel, F.: Slab break-off – abrupt cut or gradual detachment? New insights from the Vrancea Region (SE Carpathians, Romania), *Terra Nova*, 13, 172–179, 2001.

- Stein, R. S., Barka, A. A., and Dietrich, J. H.: Progressive failure on the North Anatolian fault since by 1939 by earthquake stress triggering, *Geophys. J. Int.*, 128, 594–604, 1997.
- Tavera, J.: Etude des mécanismes focaux de gros séismes et sismicité dans la région de Vrancea – Roumanie, Rapport de stage de recherche, Institut de Physique du Globe, Paris, 1991 (in French).
- Tibi, R., Wiens, D. A., and Inoue, H.: Remote triggering of deep earthquakes in the 2002 Tonga sequences, *Nature*, 424, 921–925, 2003.
- Trifu, C. I. and Radulian, M.: Frequency – magnitude distribution of earthquakes in Vrancea: Relevance for a discrete model, *J. Geophys. Res.*, 96, 4301–4311, 1991.
- Trifu, C. I., Deschamps, A., Radulian, M., and Lyon-Caen, H.: The Vrancea earthquake of May 30, 1990: An estimate of the source parameters, *Proc. of the XXIIInd ESC Gen. Ass.*, Barcelona, 1990, 1, 449–454, 1992.
- Tondi, R., Achauer, U., Landes, M., Daví, R., and Besutiu, L.: Unveiling seismic and density structure beneath the Vrancea seismogenic zone, Romania, *J. Geophys. Res.*, 114, B11307, doi:10.1029/2008JB005992, 2009.
- Turcotte, D. L. and Schubert, G.: *Geodynamics, Applications of continuum physics to geological problems*, Wiley, New York, USA, 432 pp., 1982.
- Wenzel, F., Lorenz, F., Sperner, B., and Oncescu, M. C.: Seismotectonics of the Romanian Vrancea area, in: *Vrancea Earthquakes: Tectonics, Hazard and Risk Mitigation*, edited by: Wenzel, F., Lungu, D., and Novak, O., Kluwer Academic Publishers, Dordrecht, Netherlands, 15–26, 1999.
- Wenzel, F., Sperner, B., Lorenz, F., and Mocanu, V.: Geodynamics, tomographic images and seismicity of the Vrancea region (SE-Carpathians, Romania), *EGU Stephan Mueller Special Publication Series*, 3, 95–104, 2002.
- Wells, D. L. and Coppersmith, K. J.: New empirical relationships among magnitude, rupture length, rupture width, rupture area and surface displacement, *B. Seismol. Soc. Am.*, 84(4), 974–1002, 1994.
- Wortel, M. J. R. and Spakman, W.: Subduction and slab detachment in the Mediterranean-Carpathian region, *Science*, 290, 1910–1917, 2000.